Optical rectification by ratchet transport in an asymmetric grating

Cite as: AIP Advances **11**, 115006 (2021); https://doi.org/10.1063/5.0062816
Submitted: 08 July 2021 • Accepted: 08 October 2021 • Published Online: 02 November 2021

P. Moroshkin, T. Ochiai, R. Osgood, et al.

Optical rectification by ratchet transport in an asymmetric grating

Cite as: AIP Advances 11, 115006 (2021); doi: 10.1063/5.0062816
Submitted: 8 July 2021 • Accepted: 8 October 2021 •
Published Online: 2 November 2021

P. Moroshkin,[1,a)] T. Ochiai,[2] R. Osgood III,[3] and J. Xu[1,4]

AFFILIATIONS

[1] School of Engineering, Brown University, Providence, Rhode Island 02912, USA
[2] Research Center for Functional Materials, National Institute for Materials Science, Tsukuba 305-0044, Japan
[3] Army DEVCOM SC, Natick, Massachusetts 01760, USA
[4] Department of Physics, Brown University, Providence, Rhode Island 02912, USA

[a)] **Author to whom correspondence should be addressed:** petr_moroshkin@brown.edu

ABSTRACT

We report on electron ratchet transport's manifestation in the optical rectification (OR) of an asymmetric grating. The photon-drag enabled effect is magnified by asymmetric photon scatterings and the induced optical nonlinearity associated with the surface plasmon polariton (SPP) via its near-field and gradient intensifications. The measured OR efficiency is increased multi-fold, over the prior art, which is attributable to its operating in a higher-order diffraction and nonlinearity regime and to a minimized coupling loss to a potential SPP mode at the lower interface.

Nonlinear light–matter interactions are at the root of a broad range of physical phenomena or effects that have found high impact applications in both classical and quantum optics. The second harmonic generation (SHG) and the spontaneous parametric down conversion (SPDC) or entangled photon-pair generation are prominent examples in each regime. While the interest in their uses has been expanding rapidly, the range of material choices with sufficient optical nonlinearities suitable for the applications has remained limited. Fortunately, it has been realized that an enhanced optical nonlinearity could also rise from a system with a localized and intensified electromagnetic field and its spatial gradient.[1] This opens a door to opportunities to engineer nonlinear light–matter interactions rather than solely relying on available materials. One scheme of nonlinearity engineering could be that of sub-wavelength structuring to intentionally intensify and localize the fields at structural features designed to create, add, or enhance the structural-material's nonlinearity. Surface plasmon polaritons (SPPs) of metallic nanostructures are good candidates and have indeed been shown to enhance SHG by orders of magnitude.[2] Optical Rectification (OR) is the DC counterpart of SHG. It refers to the process of generating a DC electric voltage or current in a sample irradiated with light. By itself, OR paves the way for fastest photodetection, with the electron inertia being its only speed limitation as opposed to the traditional capacitance charging or the band-to-band transitions followed by drift-diffusion. It is an external manifestation of atomic or molecular polarization in insulators or unidirectional momentum transfer to free electrons in conductors by incident light. In conductive materials, it is often termed photon drag.[3] In a metallic grating, the process is accompanied and enhanced by the excitation of surface plasmon waves.[4–8]

In a symmetric grating under normal incidence of light though, the oscillating spatial displacement of electrons averages out over time to a net zero. In an asymmetric metallic grating, a net spatial displacement is expected of the force resulting from the gradient of the electromagnetic energy density that is localized to the surface and is spatially asymmetric. This asymmetric force nudges the oscillating electrons to move more in one direction than the other, from one unit cell to the next, in a ratchet relay process. This ratchet transport can take place even with light incident at the normal (zero) angle, in which case the incoming photons bring in a zero momentum along the sample surface. Instead, the asymmetric grating provides the global "crystal momenta" and the localized field- and energy-densities with a non-zero net force in one direction. A finite DC current would result, as demonstrated in

Refs. 4, 5. Evidently, for the incidence at an oblique angle, a portion of the photon momentum can also be directly transferred to electrons via absorption and scattering—i.e., photon drag.

Conceptually, the asymmetric grating concerned here is essentially a one-dimensional lattice with a broken spatial-inversion symmetry (SIS) in its unit cell. It could be viewed as two superimposed gratings of the same period, with features of different widths, phase-shifted from each other. In this regard, one may also view it as an asymmetrically modulated charge electron density wave.[9] Relevant effects have been investigated in the THz frequency range using graphene samples.[10–12]

Earlier studies[5,13] concentrated on a regime with the grating period D approximately equal to the laser wavelength λ_{Las} for the most efficient excitation of the SPP resonance in the film. Our design of the asymmetric grating is shown in Fig. 1. On the surface, it bears a similarity to that reported in Ref. 5, but with two important differences. One is that D is approximately twice the wavelength of the incident light, λ_{Las} = 808 nm. This choice is motivated by several considerations. Relative to the 1200 nm wavelength in Ref. 5, the 808 nm light is closer to the intrinsic plasma frequency of the gold film. The grating is made of subwavelength terraces and grooves. Keeping them relatively large also makes the grating relatively more fault tolerant in a given fabrication process. More importantly, $D \approx 2\lambda_{Las}$ favors higher diffraction orders. This can be seen in the gold-air grating SPP mode wavelength dependence[14] on the structural parameters,

$$\lambda_{m'} = \frac{D}{|m'|}\mathrm{Re}\left[\sqrt{\frac{\varepsilon}{\varepsilon+1}}\right], \tag{1}$$

where ε is the frequency-dependent relative permittivity of the metal (gold).[15] At $\lambda_{m'}$ = 808 nm, the relative permittivity takes a complex value whose absolute value is much larger than 1 and the square-root term in Eq. (1) is close to unity. One could therefore expect a resonant excitation of the SPP mode of $m' = \pm 2$. One expects these diffraction orders of $m = \pm 2$ to be the more effective since they direct the scattered light more along the surface than back into the free space.

The other structural difference by design is in the thickness of the gold film. 100 nm was chosen in our case vs the 40 nm in Ref. 5. As the incident light is exponentially attenuated over the thickness, very little of it can reach the lower interface between the gold and the substrate (glass). One therefore could neglect the SPP wave at that interface, along with its coupling to the top interface, probably unlike the situation in Ref. 5.

The 1D asymmetric grating sample was produced by electron-beam lithography. The grating is formed by grooves patterned, by a lift-off process, into an 80 nm thick (H_1) Au slab atop of a 100 nm thick (H_0) continuous Au film on a glass substrate. An electron microscope (SEM) image of the fabricated grating is shown in Fig. 1, next to its cross-sectional view.

The grating consists of 100 unit cells with a period D = 1488 nm in the x-direction and a transversal dimension of 100 μm in the y-direction. The asymmetric unit cell is made of two terraces of widths $A_1 = D/2$ and $A_2 = D/5$, respectively. They are separated by grooves of the widths $B_1 = D/5$ and $B_2 = D/10$, respectively. The continuous gold film underlying the grating is electrically connected to a lock-in amplifier (input impedance 1 kΩ) for the OR current measurements.

The gold film–air interface is illuminated by a linearly polarized cw diode laser at λ_{Las} = 808 nm, focused by an F = 50 mm lens to a spot with a diameter (FWHM) of 120 μm, slightly larger than the grating. The mean laser power incident on the grating area is 50 mW. The laser beam is on–off modulated by a mechanical chopper, and the OR signal is detected at the modulation frequency. During the measurement, the polarization angle of the pump light, α, is rotated from being parallel to the y-axis (along the grooves, $\alpha = 0$) to along the x-direction (perpendicular to the grooves, $\alpha = 90°$).

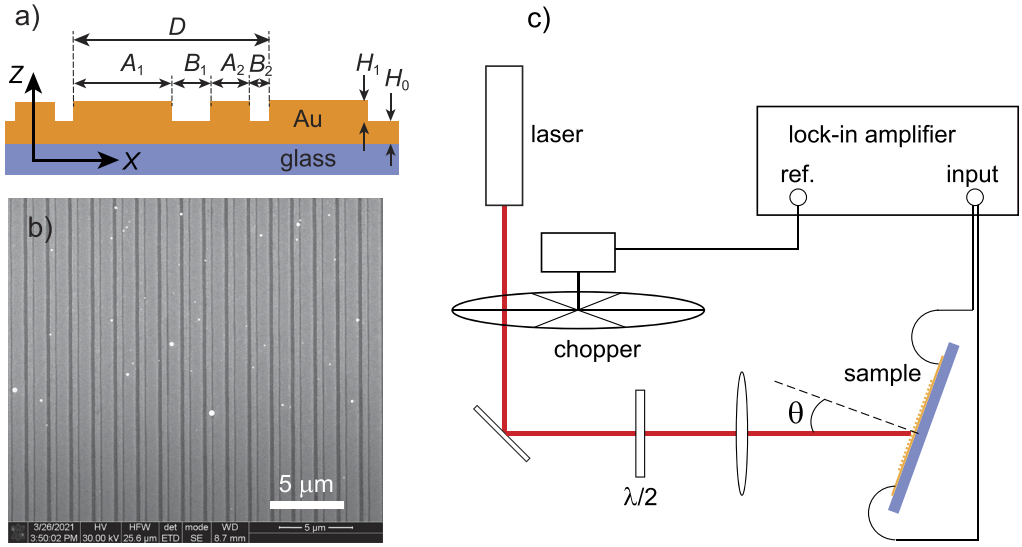

FIG. 1. A sketch (a) and an SEM image (b) of a 1D asymmetric grating used in the experiment. (c) A schematic of the experimental setup.

Figure 2(a) shows the detected OR signal at normal incidence, plotted vs the angle α. The signal amplitude exhibits a clear sinusoidal dependence, as expected. It reaches maxima at $\alpha = \pm 90°$ when the E-field is polarized across the grating lines and most effectively drives the electron oscillations across the grating structure and excites the SPP mode along the x-direction of the film.

Figure 2(c) shows the measured OR signal dependence on the angle of incidence, with a maximum signal at $\theta = 0$ (i.e., normal incidence) and at $\theta = \pm 33°$. When the incidence angle switches from $\theta < 0$ to $\theta > 0$, the rectified current remains positive instead of becoming anti-symmetric, as would occur for a symmetric grating structure.[5] In the same plot, we show the sample absorbance computed with the help of the COMSOL model. It shows three peaks at $\theta = 0, \pm 33°$, in remarkable agreement with the experimental OR data.

The maximal OR current reached 4 nA, which corresponds to an efficiency of 12 mV/(MW/cm^2). Our measured result is thus four times higher than that reported in a prior work[5] in which a nanosecond pulsed $\lambda = 1200$ nm laser with a much higher instantaneous power was deployed on a $D = 1220$ nm period grating with a larger area, $600 \times 600\ \mu$m^2.

On the ground of first principles, the asymmetric grating is expected to give rise to unidirectional electron transport, i.e., optical rectification. The finding is in agreement with the general expectation and consistent with the asymmetric diffractions of the laser light from the asymmetric grating.

The absorption and diffraction of light by the asymmetric grating were calculated with the help of a commercial finite-element solver COMSOL Multiphysics 5.5. A frequency-domain analysis is performed in a 2D geometry shown in Fig. 1(a), with a periodic boundary condition applied in the x-direction. Perfectly matched layers are placed above and below the grating to avoid non-physical reflections. The calculated intensities of diffraction orders $m = 0, \pm 1, \pm 2, \pm 3$ are plotted in Fig. 3(a) vs the angle of incidence. In Fig. 4, we also plot the spatial dependence of the electric field amplitude and the directions of all diffracted beams at $\theta = 0, \pm 33°$. The asymmetric profile of the grating leads to unequal reflections

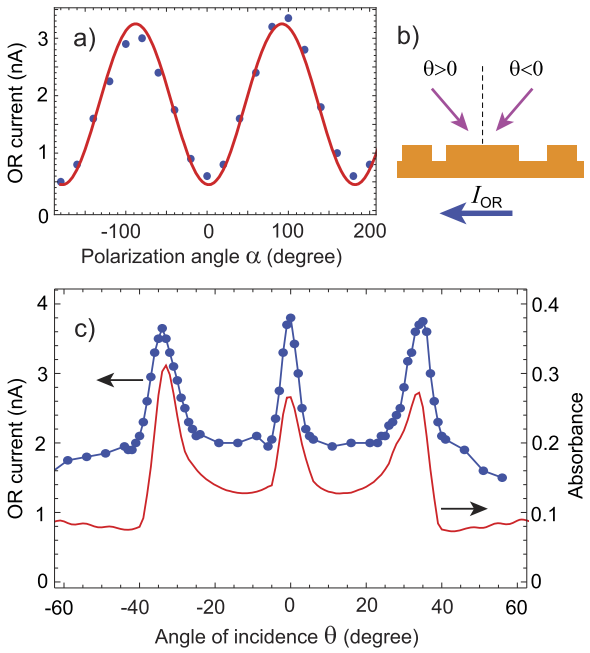

FIG. 2. Experimental optical rectification data. (a) OR signal at normal incidence, plotted vs the laser polarization angle α. (b) Cartoon showing the direction of the observed OR current with respect to the grating profile. (c) OR signal at $\alpha = 90°$, plotted vs the angle of incidence θ (blue line, left scale); theoretical absorbance curve (red line, right scale).

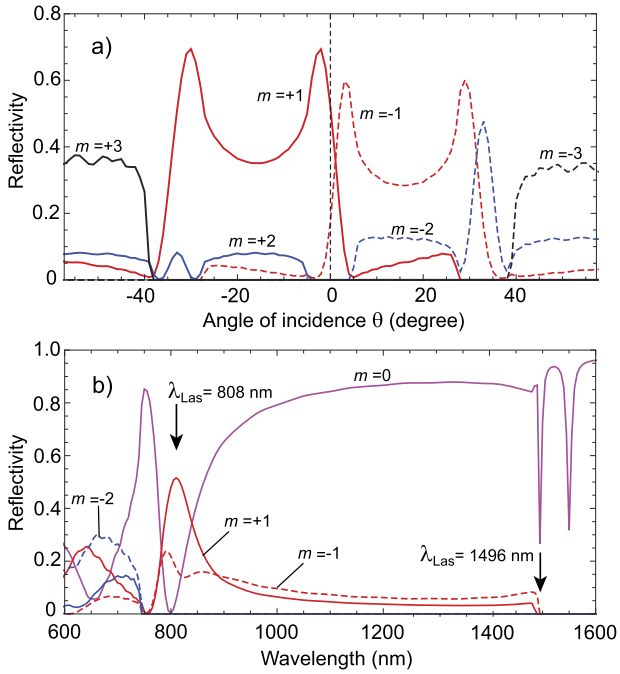

FIG. 3. Numerical COMSOL simulations of light diffraction. $D = 1488$ nm, $\alpha = 0$. (a) Intensity of diffraction orders vs the angle of incidence θ. $\lambda_{Las} = 808$ nm. (b) Reflection spectra of diffraction orders at normal incidence. Color code: magenta curve: $m = 0$, red solid curve: $m = +1$, red dashed curve: $m = -1$, blue solid curve: $m = +2$, blue dashed curve: $m = -2$, black solid curve: $m = +3$, black dashed curve: $m = -3$.

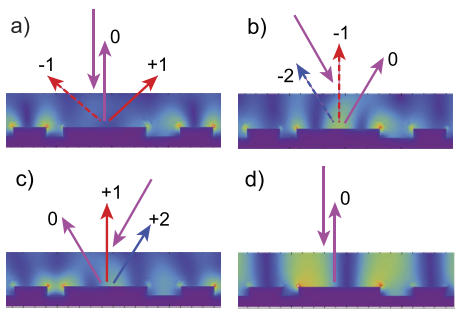

FIG. 4. Computed maps of a local electric field amplitude near the sample surface. [(a)–(c)] $\lambda_{Las} = 808$ nm, $\theta = 0, +33°$, and $-33°$. (d) $\lambda_{Las} = 1496$ nm, $\theta = 0$. The directions of the incident and diffracted light beams are shown by arrows color-coded according to Fig. 3.

of the positive and negative diffraction orders at $\theta = 0$ and to a non-symmetric dependence on θ.

The grating was designed to maximize the differences between the $m = -1$ and $m = +1$ diffraction orders for normal incident laser light of $\lambda_{Las} = 808$ nm, corresponding to a maximal momentum transfer to the electrons in the metal grating. At finite incident angles, the more conventional photon drag effect comes in to play a role as well, as seen in the reflection peaks of $m = \pm 1$ and ± 2 at $\theta = \pm 32^\circ$. These diffraction peaks lead to the maxima in the measured OR current in Fig. 2(c) at $\theta = \pm 33^\circ$. Clearly, the asymmetry remains at finite angles of incidence where direct momentum transfer takes place. The fact that the OR current direction remains the same despite the switch of the light incidence direction hints at the relative contributions from the photon drag vs the motions driven by the electromagnetic forces and nonlinearity arising from the subwavelength structuring.

Complementing the numerical and experimental findings, one can take a simplified view from the diffraction momentum conservation condition and find a qualitative or a simple principal reason in the SPP wave excitation. The diffracted and incident beams in the free space obey the condition

$$k_{Las}(\sin\theta - \sin\beta_m) = mq. \tag{2}$$

At the same time, diffraction of light on the grating structure places the excitation of the SPP under a condition

$$K_{SPP}(\omega_{Las}) = k_{Las}\sin\theta + mq, \tag{3}$$

where $K_{SPP}(\omega_{Las})$ is the wave vector of SPP at the laser frequency, $k_{Las} = 2\pi/\lambda_{Las}$ is the laser wave vector, $q = 2\pi/D$ is the grating "crystal momentum," and β_m is a diffraction angle of the order m. Since $K_{SPP}(\omega_{Las})$ is always larger than k_{Las}, the crystal momentum of the grating is required to provide the momentum conservation. At a normal incidence, this leads to $mq = K_{SPP}$ ($>k_{Las}$). Since q in our structure is roughly half of that of the 808 nm incident wave, the corresponding diffraction order $|m|$ would be 2 or more to excite a SPP mode at normal incidence. Indeed, in Figs. 4(a)–4(c), one can see that the spatial distribution of the electric field amplitude along the grating surface has four nodes in a unit cell corresponding to the SPP mode $m = 2$.

In order to compare the regimes with $\lambda_{Las} \approx 2D$ and $\lambda_{Las} \approx D$ for our particular grating design, we plot in Fig. 3 (b) the reflectivity spectra at normal incidence, computed using COMSOL. At $\lambda_{Las} = 808$ nm, the reflectivity of the zero order is close to zero and $m = +1$ has a maximum, approaching 0.55. The imbalance between $m = -1$ and $m = +1$ due to the grating asymmetry also reaches its maximum, leading to a maximized momentum transfer from diffracted photons to the sample. At the same time, the orders $m = \pm 2$ are not reflected. The corresponding condition (2) can be fulfilled only at $|\theta| \geq 5^\circ$ [see Fig. 3(a)]. However, Eq. (3) is fulfilled at $\theta = 0$ and $m = 2$, which leads to the SPP excitation and OR current enhancement.

On the other hand, at $\lambda_{Las} \approx D$, the diffraction orders $m = \pm 1$ propagate nearly parallel to the grating. Due to their unequal intensities, a net momentum is transferred to the sample and therefore some OR current can be generated. However, at $\lambda_{Las} \approx D$, the diffraction is completely dominated by the zeroth order with only a minor fraction of the photons going into the $m = \pm 1$ orders, thus greatly diminishing the momentum transfer. Under these conditions, the SPP is not excited. In order to fulfill Eq. (3) for the SPP excitation by setting $K_{SPP} = q$, one has to choose $k_{Las} < q$, which corresponds to $\lambda_{Las} > D$ with no diffraction into the free space. Indeed, the two sharp resonances observed in Fig. 3(b) at 1496 and 1550 nm correspond to the most efficient excitation of two different SPP modes at the upper surface of the grating. One of them is shown in Fig. 4(d). The non-diffraction regime of the optical rectification (photon drag)[13] lies beyond the scope of the present work.

These principal reasonings are also consistent with a Rigorous Coupled-Wave Analysis (RCWA) we performed, in which the reflectance, absorbance, and the rectification current were calculated for the same sample structure pumped by a normal incident light with a wavelength equal either to 808 or to 1616 nm. The findings qualitatively agree with the longer wavelength light having a lower absorbance and a lower OR current at normal incidence. We opt to leave a quantitative comparison to future work when we have a more precise knowledge of the structural and material parameters or control over them.

A qualitative assessment offers the advantage of focusing on principal questions such as the following: if the non-inversion symmetry and second-order nonlinearity that are essential for SHG, OR, and SPDC could be created in materials with inversion symmetry and with little or non-native nonlinearity and how they can be enhanced by what means.

Although conceptually it has been established that the spatial gradient of a localized asymmetric energy distribution could on its own lead to SHG, even in a material with a low or zero $\chi^{(2)}$ such as gold, what structural parameters or mechanisms matter, or matter more, is usually not so self-evident. In this light, the present study may be viewed as one that attempts to reach beyond the desire of achieving a higher performance in optical rectification. It represents effort in a more basic quest—engineering light–matter interactions. It shows that one could proceed in such a quest via identifying previously un- or under-explored degrees of freedom and assessing their effects in enhancing the optical nonlinearity of the entire system, rather than that of the constituent materials.

It is worth to mention another possibility of optical rectification that was made in the THz range in graphene.[10] It revealed additional mechanisms for ratchet transport: thermoratchet or Seebeck ratchet arising from spatially periodic heating of the electron gas. This mechanism is independent of the light polarization and therefore contributes little or nothing to the results shown in Fig. 2. In addition, the thermal gradient is negligibly small in our sample as its grating area is relatively small, $100 \times 150\ \mu m^2$, which was entirely covered by the pump light.

We have demonstrated infrared optical rectification arising from electron ratchet transport in a 1D asymmetric grating, which could be viewed as the superposition of two gratings of the same period. The two gratings, however, are spatially shifted by 1/5 of their period with respect to each other, thereby effectively forming a grating with a non-centrosymmetric unit cell. The OR current reached a maximum at the normal incidence, as expected in such grating structures with a broken inversion symmetry. Operationally, the structure together with the experimental setup was made to favor high order diffractions at normal incidence, which therefore resulted in a greater photon energy and momentum absorption and transfer to the horizontal direction. Underlying the optical

rectification and improved performance is a large second-order optical nonlinearity created in a material that has little or none and a non-inversion symmetry by structural engineering that converts the incident plane wave into a localized, intensified, asymmetric SPP field. As a result, the light driven electron oscillations in the grating average out over time by the asymmetric unit cell to a net or rectified drift (ratchet) motion of electrons that relays from one unit cell to another across the grating. The measured current shows a fourfold increase in efficiency over the prior record. It is attributable to the chosen pump wavelength being half of the grating period and also being closer to that of the plasma frequency of the hosting gold metal and to the suppression or near-complete elimination of the SPP modes at the lower interface between gold and glass. The asymmetric grating studied here could be further engineered to acquire even greater functionalities and performances, now that the underlying mechanisms are better understood. For example, a designer's asymmetry and local-field intensification could be achieved conceptually via the so-called binary super-grating approach studied two decades earlier.[16–18] Perhaps more meaningful is that this work represents yet another confirmation, through a specific demonstration, that optical nonlinearity could be created in a material with little or none of its own or greatly enhanced over its native value.

This exploration drew inspiration from Professor Shur's work[9] on helicity-driven ratchet transport and is enabled by AFOSR (Grant No. FA9550-19-1-0355). Spectroscopy was done by efforts in ARO, Grant Nos. W911NF-14-2-0075 and W911NF2110181.

AUTHOR DECLARATIONS

Conflict of Interest

The authors have no conflicts of interest.

DATA AVAILABILITY

The data that support the findings of this study are available from the corresponding author upon reasonable request.

REFERENCES

[1] N. Bloembergen, R. K. Chang, S. S. Jha, and C. H. Lee, Phys. Rev. **174**, 813 (1968).
[2] Y. Pu, R. Grange, C.-L. Hsieh, and D. Psaltis, Phys. Rev. Lett. **104**, 207402 (2010).
[3] J. H. Strait, G. Holland, W. Zhu, C. Zhang, B. R. Ilic, A. Agrawal *et al.*, Phys. Rev. Lett. **123**, 053903 (2019).
[4] H. Kurosawa, S. Ohno, and K. Nakayama, Phys. Rev. A **95**, 033844 (2017).
[5] T. Hatano, B. Nishikawa, M. Iwanaga, and T. Ishihara, Opt. Express **16**, 8236 (2008).
[6] N. Noginova, V. Rono, F. J. Bezares, and J. D. Caldwell, New J. Phys. **15**, 113061 (2013).
[7] M. Durach and N. Noginova, Phys. Rev. B **93**, 161406(R) (2016).
[8] A. English, C.-W. Cheng, L. Lowe, M.-H. Shih, and W. Kuang, Appl. Phys. Lett. **98**, 191113 (2011).
[9] I. V. Rozhansky, V. Y. Kachorovskii, and M. S. Shur, Phys. Rev. Lett. **114**, 246601 (2015).
[10] P. Olbrich, J. Kamann, M. König, J. Munzert, L. Tutsch, J. Eroms *et al.*, Phys. Rev. B **93**, 075422 (2016).
[11] D. V. Fateev, K. V. Mashinsky, O. V. Polischuk, and V. V. Popov, Phys. Rev. Appl. **11**, 064002 (2019).
[12] T. Ochiai, J. Opt. Soc. Am. B **34**, 740 (2017).
[13] H. Kurosawa, T. Ishihara, N. Ikeda, D. Tsuya, M. Ochiai, and Y. Sugimoto, Opt. Lett. **37**, 2793 (2012).
[14] H. F. Ghaemi, T. Thio, D. E. Grupp, T. W. Ebbesen, and H. J. Lezec, Phys. Rev. B **58**, 6779 (1998).
[15] A. D. Rakic, A. B. Djurisic, J. M. Elazar, and M. L. Majewsky, Appl. Opt. **37**, 5271 (1998).
[16] D. Levner, M. F. Fay, and J. M. Xu, IEEE J. Quantum Electron **42**, 410 (2006).
[17] D. Levner, M. F. Fay, and J. M. Xu, "Synthesis of supergratings by Fourier methods," U.S. patent 6415081 B1, Canadian patent 2382645, Australian patent 0065510, European patent 1206717 (2 July 2002).
[18] D. Levner, M. F. Fay, and J. M. Xu, "Method and apparatus for detecting multiple optical wavelengths," U.S. patent 7496257 (24 Feb. 2009).